Research Article

International Journal of Chemistry and Aquatic Sciences (IJCA)
Vol.11.Issue.1.2025(Jan-March), Page: 1-19
ISSN: 2355-033X
http://chemistryjournal.kypublications.com/

Design and Application of Kaolin-Supported Cu-ZnO Nanocomposites for Effective Removal of RM21 Dye from Aqueous Solutions

Dr. G. N. Hima Bindu
Department of Chemistry, ANU, India
Email: kvsghb2122@gmail.com

doi: 10.33329/ijca.11.1.1

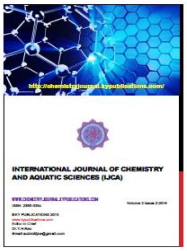

Article info
Article Received:16/01/2025
Article Accepted:19/02/2025
Published online:23/03/2025

ABSTRACT
The present study investigates the adsorption of RM21 dye from aqueous solutions using a kaolin-supported copper-doped zinc oxide (Cu-ZnO) nanocomposite as an effective adsorbent. The nanocomposite was synthesized and characterized using SEM-EDX and FT-IR techniques to confirm the morphology, elemental composition, and functional groups before and after adsorption. Adsorption experiments were conducted to evaluate the effects of contact time, initial dye concentration, and adsorbent dosage on the removal efficiency. The equilibrium data were analyzed using multiple isotherm models, including Langmuir, Freundlich, Temkin, Jovanovich, Halsey, and Redlich-Peterson, revealing that the Redlich-Peterson model best described the adsorption behavior, indicating heterogeneous surface interactions. Kinetic studies demonstrated that the adsorption process followed a pseudo-second-order model with high correlation (R^2 = 0.9999), suggesting chemisorption as the dominant mechanism. Thermodynamic parameters (ΔG°, ΔH°, and ΔS°) indicated that the adsorption was spontaneous, endothermic, and feasible under experimental conditions. The study confirms that kaolin-supported Cu-ZnO nanocomposite is a promising, efficient, and environmentally friendly adsorbent for the removal of reactive dyes from wastewater. This work provides insights into the practical application of nanocomposite materials for dye-contaminated water treatment.

Keywords: Adsorption, RM21 dye, Cu-ZnO nanocomposite, Kaolin, Kinetics, Isotherms

.

Introduction

In recent years, rapid population growth and industrialization have led to negative impacts on the environment and the depletion of natural resources. As a consequence of industrialization, the release of various pollutants into the environment has reduced environmental quality. Industrial wastes, wastewater, heavy metals, synthetic agricultural fertilizers, detergents, pesticides, and dyes

used in the textile industry are among the many factors that disrupt natural balance (Markandeya et al., 2022; Velusamy et al., 2021; Xu et al., 2020; Mia et al., 2019). Textile industries use dyes to color their final products and generate large amounts of waste containing organic matter and color (Lellis et al., 2019). The presence of these substances with complex aromatic structures negatively affects aquatic environments by reducing photosynthetic activity. Furthermore, many of these aromatic compounds cause skin irritation and respiratory problems, while also increasing the risks of cancer and cell mutation in humans. Therefore, wastewater containing dyes must undergo effective treatment before being discharged into the environment (Al-Tohamy et al., 2022; Hassan & Carr, 2018).

Reactive dyes are a class of dyes widely used in textiles for coloring various fibers, particularly cellulosic fibers, as well as wool, silk, and polyamide. Their high fastness, simple application methods, and ability to provide all colors in the visible spectrum make reactive dyes stand out, especially in cotton, which is the most important member of the cellulosic fiber group (Özdemir & Tutak, 2016). Reactive dyes are considered an important class of dyes for cotton due to their favorable fastness properties, particularly wash fastness. A covalent bond forms between the functional groups of the dye molecule and the hydroxyl groups on the cellulosic fiber. However, in the dyeing medium, reactive dyes undergo a hydrolysis reaction with water molecules, losing their ability to dye fibers, which is regarded as their main disadvantage (Ghaffar et al., 2019; Bamfield, 2001; Broadbent, 2001).

Reactive Blue 21 (RM21), with the molecular formula $C_{40}H_{25}CuN_9O_{14}S_5$, is widely used in the textile industry due to its properties such as high stability, optimal solubility, and long shelf life (Aksu & Isoglu, 2007; Vaghela & Nath, 2020). Because of its highly stable aromatic structure, it is difficult to degrade RM21 dye. The discharge of RM21 dye from various textile industries into water sources poses a serious concern due to its non-biodegradability, toxicity, and mutagenicity. Consequently, it harms the ecosystem by causing the death of living organisms. The chemical structure of RM21 dye is shown in Figure 1 (Ahmad et al., 2019).

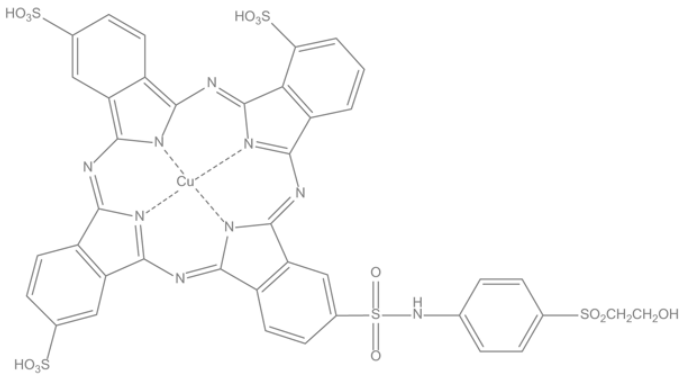

Figure 1. Chemical structure of RM21 dye

Various methods such as coagulation/flocculation, membrane filtration, reverse osmosis, photodegradation, ozonation, and adsorption are used for the removal of dyes from wastewater (Liu et al., 2019; Bilińska et al., 2019; El-Bindary et al., 2016; Luo et al., 2022; Kızıltaş, 2022; Tekin et al., 2020). Each of these methods has its own advantages and disadvantages. Among them, adsorption is the most preferred technique because it is easy to apply, highly efficient, less complicated than other conventional methods, cost-effective, and environmentally friendly (Senthil Rathi & Senthil Kumar, 2021; De Gisi et al., 2016). A wide variety of adsorbents have been employed for dye removal from wastewater through adsorption. Activated carbon, alumina, zeolites, and silica gel are some of the commercially used adsorbents. Although these adsorbents generally meet the expectations in terms of adsorption capacity, there is still a need to develop adsorbent materials with both high adsorption capacity and low cost. Therefore, many research groups continue laboratory studies in this field

(Hamad & Idrus, 2022; Nasar & Mashkoor, 2019; Bayramoğlu et al., 2020; Zhou et al., 2019; Yagub et al., 2014).

Recently, studies on the use of nanostructured metal oxides as adsorbents have been increasing due to their small particle size, large surface area, and high number of active sites (Sun et al., 2012; Naseem & Durrani, 2021). The adsorption capacity of these nanometal oxides has been enhanced by decorating them onto various supporting surfaces such as clay, zeolite, activated carbon, graphene, and carbon nanotubes (Kibanova et al., 2012; Alswat et al., 2022; Pala et al., 2022; Gan et al., 2019). Owing to the synergistic effect of such nanometal composites, they exhibit higher adsorption capacities compared to individual metal oxides (Eskandari et al., 2021; Ayanda et al., 2013; Lu & Chiu, 2006). Nanometal oxides such as cadmium sulfide, tungsten trioxide, titanium oxide, and zinc oxide are the most commonly preferred for nanocomposite synthesis because of their low cost, high surface area, good stability, low toxicity, long-term durability, and excellent adsorption capacity (Mahmood, 2022; Patra et al., 2022; Chandrabose et al., 2021; Binaeian et al., 2020; Stengl & Krˇalová, 2011; Muthuvela et al., 2020).

Clays such as kaolin, bentonite, and montmorillonite are widely used as primary supports in nanocomposite synthesis (Ewis et al., 2022; Fadillah et al., 2020). Kaolin, due to its high thermal stability, good surface area, and layered structure, is one of the most preferred clays for the synthesis of clay-supported nanocomposites. The distribution of nanometal oxides on the kaolin surface reduces aggregation and particle size compared to their pure forms, while providing a suitable support surface. As a result, kaolin-supported nanocomposites demonstrate improved adsorption capacity (Khan et al., 2015; Rind et al., 2023).

In this study, the removal of RM21 dye, commonly used in the textile industry, was investigated through the adsorption method using a copper-doped zinc oxide nanocomposite decorated on kaolin. Various parameters such as initial dye concentration, adsorbent dosage, temperature, and contact time were optimized to determine the most suitable conditions for the removal of RM21 dye. Furthermore, adsorption isotherms, kinetic, and thermodynamic data were obtained and evaluated.

2. Materials and Methods

2.1. Materials

For adsorption studies, Reactive Blue 21 (Sigma-Aldrich) dye was obtained in solid powder form. Stock solutions were prepared, and the necessary dilutions were made to obtain the desired dye concentrations. Deionized water was used in the preparation of all solutions.

2.2. Synthesis of Copper-Doped ZnO Nanocomposite Decorated on Kaolin Surface

The copper-doped ZnO nanocomposite decorated on kaolin, used as an adsorbent, was synthesized by the co-precipitation method. The synthesis procedure has been described in detail in our previous study (Keleş Güner & Çağlar, 2020).

2.3. Adsorption Study

Adsorption experiments for the removal of RM21 dye using the previously synthesized copper-doped ZnO nanocomposite decorated on kaolin were carried out on a magnetic stirrer to ensure homogeneous mixing (Keleş Güner & Çağlar, 2020). To determine the contact time, dye and adsorbent solutions with the same initial RM21 concentration (25 mg L^{-1}), adsorbent dosage (30 mg L^{-1}), and temperature (25 °C) were placed in separate flasks at their natural pH (pH 7) and stirred on a magnetic stirrer. At specific time intervals (0–120 min), the residual dye concentration was measured using a UV-Vis spectrophotometer (PG Instruments T80+). After determining the equilibrium time, the effects of

initial RM21 concentration, adsorbent dosage, and temperature on adsorption were investigated. Spectrophotometric measurements were performed at the maximum absorption wavelength of RM21 dye (666 nm). A calibration curve, obtained by plotting absorbance values against known concentrations, was used to determine the remaining dye concentrations in the solution.

In the adsorption experiments, initial dye concentrations of 15, 25, and 35 mg L^{-1} were studied, while adsorbent dosages were varied as 5, 10, 15, 20, 25, 30, and 35 mg L^{-1}. Temperature studies were carried out at 25, 35, and 45 °C. During the experiments, samples were withdrawn at specified intervals and centrifuged at 5000 rpm for 3 minutes to separate the particles from the mixture. The supernatant was then analyzed by spectrophotometry to determine the remaining RM21 concentration. Sampling and analyses continued until equilibrium was reached.

The percentage removal (% Removal) and equilibrium adsorption capacity (qe) were calculated using Equations (1) and (2) (Kumbhar et al., 2022):

$$\%\text{Removal} = \frac{(C_o - C_e)}{C_o} \times 100$$

$$q_e = \frac{(C_o - C_e) \times V}{M}$$

where Co and Ce (mg L^{-1}) are the initial and equilibrium dye concentrations, respectively, V(L) is the solution volume, and M (g) is the mass of the adsorbent.

2.4. Characterization

The characterization of the synthesized sample was discussed in detail in our previous publication (Keleş Güner & Çağlar, 2020). After adsorption of the RM21 dye, SEM-EDX and FT-IR analyses were performed and discussed in Section 3.5. SEM/EDX analyses were carried out using a field emission scanning electron microscope (Quanta FEG 450-FEI), while FTIR spectra were recorded using a Thermo Nicolet 6700 spectrophotometer in the range of 4000–400 cm^{-1} with a resolution of 4 cm^{-1}.

3. Results and Discussion

3.1. Effect of Adsorption Parameters

3.1.1. Effect of Adsorbent Dosage

The amount of adsorbent used has a significant effect on the removal of RM21 dye. The effect of adsorbent dosage was studied at an initial RM21 concentration of 25 mg L^{-1} and a temperature of 25°C, with the adsorbent dosage varying from 5 mg L^{-1} to 35 mg L^{-1}. As shown in Figure 2, the dye removal efficiency gradually increased with increasing adsorbent dosage. When 5 mg L^{-1} of adsorbent was used, RM21 removal was 16.1%, whereas increasing the dosage to 35 mg L^{-1} increased the removal to 97.2%. The increase in adsorbent dosage enhances the number of active surface sites available for adsorption, thereby increasing the amount of dye adsorbed per unit mass of adsorbent. Since nearly complete dye removal was achieved at an adsorbent dosage of 35 mg L^{-1}, a slightly lower dosage of 30 mg L^{-1} was selected for subsequent kinetic and thermodynamic studies to maintain efficiency while optimizing material use.

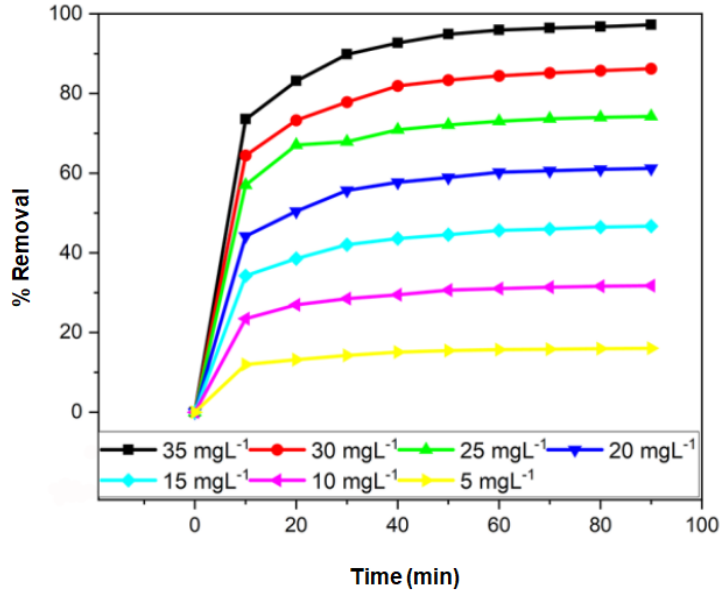

Figure 2. Effect of adsorbent dosage on RM21 removal using copper-doped ZnO nanocomposite decorated on kaolin

3.1.2. Effect of Initial RM21 Dye Concentration

To investigate the effect of initial RM21 concentration, experiments were carried out at solution pH 7, adsorbent dosage 30 mg L^{-1}, temperature 25°C, and initial dye concentrations of 15, 25, and 35 mg L^{-1}. The results are shown in Figure 3. Increasing the initial dye concentration reduced the adsorption capacity of the copper-doped ZnO nanocomposite decorated on kaolin, resulting in lower dye removal (Kul et al., 2022). When the initial dye concentration decreased from 35 mg L^{-1} to 15 mg L^{-1}, RM21 removal increased from 73.1% to 96.2%. This decrease in adsorption at higher dye concentrations is attributed to the saturation of the active sites on the adsorbent surface. Additionally, higher dye concentrations in solution promote dye aggregation, reducing the available binding capacity at adsorption sites, while lower concentrations allow rapid mass transfer and efficient adsorption due to minimal molecular interactions (Demir & Kalpaklı, 2020). Since nearly complete removal was achieved at 15 mg L^{-1}, an intermediate initial dye concentration of 25 mg L^{-1} was chosen for subsequent kinetic and thermodynamic studies to ensure efficient and consistent results.

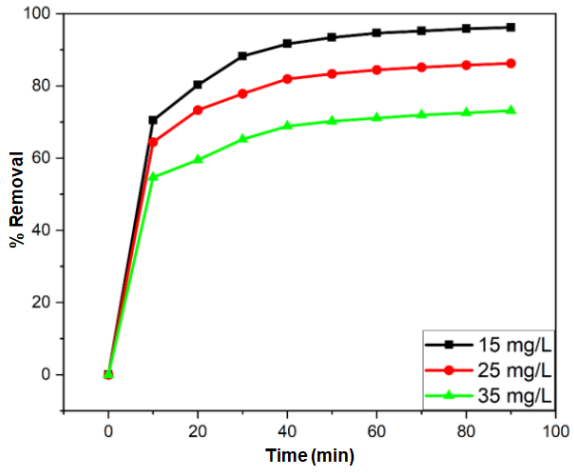

Figure 3. Effect of initial dye concentration on RM21 removal using copper-doped ZnO nanocomposite decorated on kaolin

3.1.3. Effect of Temperature

Temperature is one of the most critical factors influencing the adsorption process. Changes in temperature can affect the solubility of the pollutant in water and, consequently, the extent of its removal. To determine the effect of temperature on RM21 removal, the adsorbent dosage was fixed at 30 mg L^{-1} and the initial dye concentration at 25 mg L^{-1}, while adsorption efficiency was measured at different temperatures (25, 35, and 45°C). As shown in Figure 4, the adsorption capacity of RM21 on the copper-doped ZnO nanocomposite decorated on kaolin increased with temperature. This indicates that the adsorption of RM21 from aqueous solution onto the nanocomposite surface is likely an endothermic process (Bensalah et al., 2021). At 90 minutes, the dye removal efficiency increased from 86.22% at 25°C to 97.61% at 45°C.

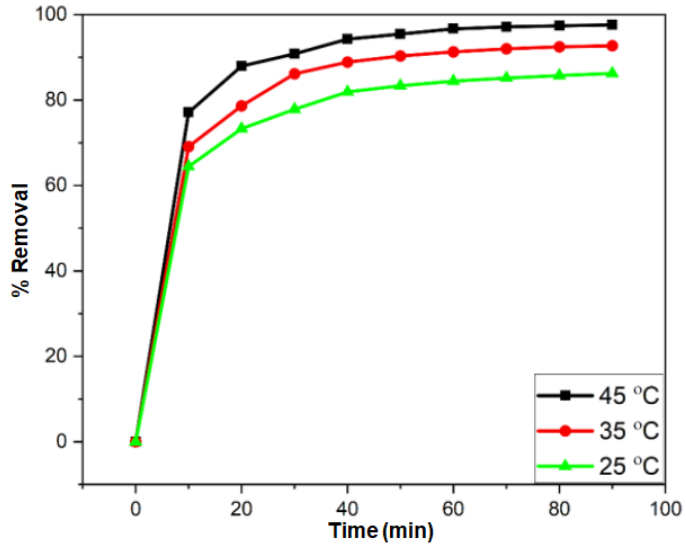

Figure 4. Effect of temperature on RM21 removal using copper-doped ZnO nanocomposite decorated on kaolin

3.2. Adsorption Isotherms

Adsorption isotherms, which are important both theoretically and practically, describe the relationship between the amount of a substance adsorbed and its concentration in solution at equilibrium and at a constant temperature. Generally, adsorption isotherms explain how adsorbates interact with adsorbents. Correlating equilibrium data with a theoretical or empirical equation is essential for the practical design and operation of an adsorption system (Karaoğlu et al., 2009; Alkan et al., 2005). Numerous isotherm models exist, and in this study, the Langmuir, Freundlich, Temkin, Jovanovich, Halsey, and Redlich-Peterson models were selected.

3.2.1. Langmuir Isotherm

The Langmuir isotherm is derived under the assumption that the adsorbent surface contains equivalent active sites and describes monolayer adsorption on a homogeneous surface. The linearized mathematical form of the Langmuir adsorption isotherm is expressed as follows (Küçük, 2021; Zheng et al., 2013):

$$\frac{C_e}{q_e} = \frac{1}{q_m} C_e + \frac{1}{q_m K_L}$$

Here, by plotting Ce/qe versus Ce, the monolayer adsorption capacity qm is determined from the slope, and the Langmuir constant K_L is determined from the y-intercept (**Figure 5a**). K_L represents the

Langmuir constant (L ·mg^{-1}), and qmq_mqm represents the maximum monolayer adsorption capacity of the adsorbent.

According to the Langmuir model, the adsorption of RM21 onto the copper-doped ZnO nanocomposite decorated on kaolin showed a correlation coefficient R2R^2R2 of 0.9994. The monolayer adsorption capacity qmq_mqm was 40.48 mg ·g^{-1}, and the Langmuir constant K_L was 2.35 (Table 1). Experimentally, the highest adsorption capacity was determined as 40 mg ·g^{-1} at 25°C after 90 minutes using 5 mg ·L^{-1} of the nanocomposite. This shows that the experimentally observed maximum adsorption capacity is in good agreement with the Langmuir isotherm prediction (Bayramoğlu et al., 2009).

The dimensionless separation factor R_L is used to evaluate the favorability of adsorption (Equation 4). R_L >1 indicates unfavorable adsorption, R_L =1 linear, 0< R_L<1 favorable, and R_L R_L =0 irreversible (Sarı & Soylak, 2006):

$$R_L = \frac{1}{1 + K_L C_0}$$

Here, R_L is the separation factor. The obtained R_L values for dye concentrations ranging from 15–35 mg ·L^{-1} were between 0.92–0.98, indicating favorable adsorption of RM21 onto the copper-doped ZnO nanocomposite decorated on kaolin.

3.2.2. Freundlich Isotherm

The Freundlich isotherm assumes a heterogeneous distribution of active sites and supports multilayer adsorption (Kalam et al., 2021). This empirical model assumes that stronger binding sites are occupied first, and as more sites are occupied, the binding strength decreases. The linear form of the Freundlich equation is given as follows (Kumbhar et al., 2022; Ncibi et al., 2007):

$$\ln q_e = \ln K_F + \frac{1}{n} \ln C_e$$

By plotting lnqe versus lnCe (**Figure 5b**), the slope gives 1/n1/n1/n, and the y-intercept gives K_F relates to the adsorption capacity for multilayer adsorption, and nnn indicates adsorption intensity depending on adsorbent heterogeneity. If n<1, adsorption intensity is suitable for the studied concentration range; if n>1, adsorption intensity is more suitable for higher concentrations. The heterogeneity factor 1/n ranges from 0–1; the closer to zero, the more heterogeneous the surface (Eren et al., 2010). A 1/n value below 1 represents a normal Langmuir-type adsorption, while above 1 indicates cooperative adsorption (Alkan et al., 2005).

For RM21 adsorption onto the copper-doped ZnO nanocomposite decorated on kaolin, the obtained 1/n value was 0.0452, indicating the surface heterogeneity of the composite. Based on the correlation coefficients (R^2), adsorption was better described by the Langmuir model than by the Freundlich isotherm (Nandi et al., 2009; Rais, 2009).

3.2.3. Temkin Isotherm

The Temkin isotherm considers the adsorption heat of all molecules in solution and is expressed as follows (Zewde & Geremew, 2022):

$$q_e = \frac{RT}{b} \ln K_T + \frac{RT}{b} \ln C_e$$

As shown in **Figure 5c**, a plot of qe versus lnCe allows the determination of *b* from the slope and K_T from the y-intercept. Here, T is the temperature (K), RRR is the universal gas constant (J ·mol^{-1} ·K^{-1}), *b* is the adsorption enthalpy (J ·mol^{-1}), and K_T is the equilibrium binding constant (L ·g^{-1}).

In an adsorption process, as the surface coverage of the adsorbent increases, the heat of adsorption of the adsorbent molecules decreases linearly. This occurs due to interactions between the adsorbate molecules and the adsorbent surface. The Temkin model is useful for determining the heat reduction during adsorption and allows the estimation of the binding energy of the reaction (Demir et al., 2022). As seen in Table 1, with a correlation coefficient R^2 of 0.9337, the Temkin isotherm model effectively describes the decrease in adsorption heat for RM21 adsorption onto the copper-doped ZnO nanocomposite decorated on kaolin.

3.2.4. Jovanovich Isotherm

The Jovanovich isotherm, similar to the Langmuir model, describes monolayer adsorption but also assumes that interactions between adsorbate and adsorbent are significant, unlike the Langmuir model (Kiełbasa et al., 2021; Saloğlu, 2019). The linear form of the Jovanovich isotherm is:

$$\ln q_e = \ln q_m - K_J C_e$$

As shown in **Figure 5d**, plotting $\ln q_e$ versus Ce allows determination of the Jovanovich constant K_J from the slope and the maximum monolayer adsorption capacity q_m from the y-intercept. Here, K_J is the Jovanovich constant, and q_m represents the maximum monolayer adsorption capacity of the adsorbent.

This model has limited application in physical adsorption. This model is applicable to situations where there are no real interactions between adsorbate molecules on mobile, monolayer surfaces. If the adsorbate concentration is high, it may be possible to reach a saturation point. On the other hand, at low adsorbate concentrations, this model reduces to Henry's law. Compared to the Langmuir model, the Jovanovich model exhibits a slower approach to saturation (Al-Ghouti and Da'ana 2020). As can be seen from the R2 value of 0.9441, the adsorption data of RM21 dye onto a copper-doped zinc oxide nanocomposite decorated on a kaolin surface matched the Jovanovich model.

Table 1. Isotherm parameters for RM21 adsorption on copper-doped ZnO nanocomposite decorated on kaolin (Conditions: contact time 90 min, initial dye concentration 25 mg L^{-1}, adsorbent dosage 30 mg L^{-1}, temperature 25°C).

Model	**Parameter**	**Value**
Langmuir	Qm (mg·g^{-1})	40.48
	KL (L·mg^{-1})	2.35
	RL	0.94
	R^2	0.9994
Freundlich	1/n	0.0452
	n	22.12
	KF (mg·g^{-1})(L·mg^{-1})$^{1/n}$	34.48
	R^2	0.942
Temkin	b (J·mol^{-1})	1477.1
	KT (L·g^{-1})	7.78×10^{8}
	R^2	0.9337
Jovanovich	KJ	-0.0071

	qm (mg $\cdot g^{-1}$)	35.02
	R^2	0.9441
Halsey	n	-22.12
	KH	9.57×10^{-35}
	R^2	0.942
Redlich-Peterson	β	0.9548
	A	34.48
	R^2	0.9999

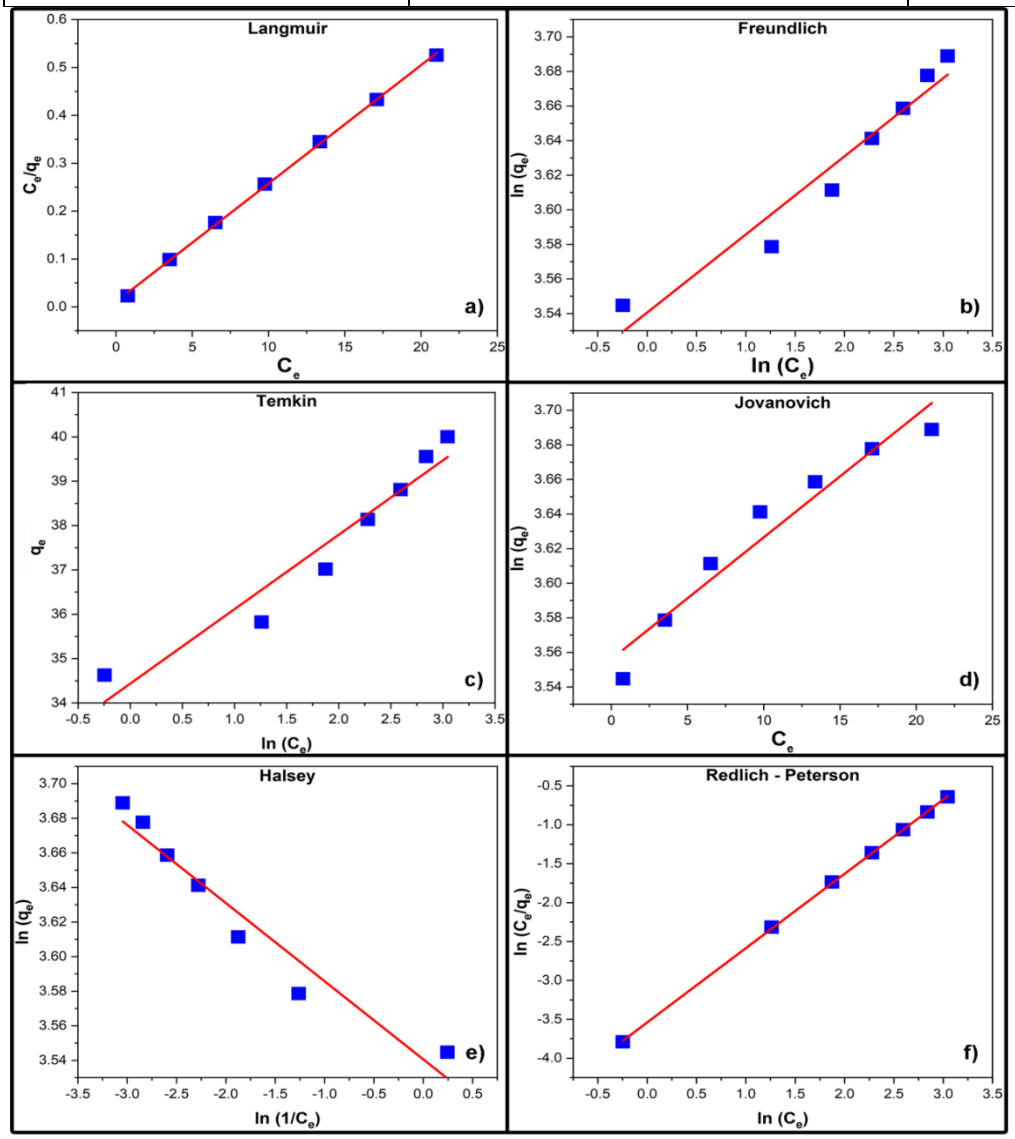

Figure 5. Linear plots of different isotherm models (a) Langmuir (b) Freundlich (c) Temkin (d) Jovanovich (e) Halsey (f) Redlich-Peterson.

3.3. Adsorption Kinetics

Kinetic studies are important to understand the mechanism by which adsorbate removal occurs. It is an important step in revealing the adsorption steps that affect the rate of the adsorption process

(Kumbhar et al. 2022, Özdemir 2015). Experimental results were studied according to pseudo-first-order, pseudo-second-order, intraparticle diffusion, and Elovich kinetic models.

3.3.1 Pseudo-First-Order Kinetics

The pseudo-first-order kinetic model was developed by Lagergren and is expressed as follows (Lagergren 1898, Nazifa et al. 2017):

$ln(qe-qt)=lnqe-k1t$ (10)

Here, qt is the amount of substance adsorbed per unit mass of adsorbent at any instant (mgg-1), k1 is the pseudo-first-order kinetic rate constant (min-1), and t is the contact time. As shown in Figure 6a, the change in the ln(qe-qt) value against time is plotted to obtain the k1 and theoretical qe values. The rate constant k1 is calculated from the slope, and the theoretical qe is calculated from the point where the line intersects the y-axis of the graph. The rate constant, maximum adsorption capacity, and correlation coefficient values are shown in Tables 2 and 3. These were obtained by plotting ln(qe-qt) against contact time, as shown in Figure 6a.

In Tables 2 and 3, it is clear that the calculated and theoretical qe (mg/g) values for the Pseudo-First-Order Kinetic model do not match each other. Furthermore, the correlation coefficient (R2) values are lower than those for the Pseudo-Second-Order Kinetic model, indicating that the adsorption data fit the Pseudo-First-Order kinetic model poorly.

3.3.2. Pseudo-Second-Order Kinetic

The Pseudo-Second-Order kinetic model is expressed as follows (Saeed et al. 2022).

$tqt=1k2qe2+tqe$ (11)

Here, k2 is the pseudo-second-order kinetic rate constant (min-1). As in Figure 6b, the change in the tqt-1 value against time is plotted and the k2 and theoretical qe values are obtained graphically. Theoretical qe is calculated from the slope, and k2 is calculated from the point where the line intersects the y-axis of the graph.

The rate constant, maximum adsorption capacity, and correlation coefficient values are shown in Tables 2 and 3.

Table 2. Effect of adsorbent dosage on kinetic parameters for RM21 adsorption on copper-doped ZnO nanocomposite decorated on kaolin

(Conditions: contact time: 90 min, initial dye concentration: 25 mg·L⁻¹, temperature: 25°C)

Kinetic Model	Parameter	5 mg	10 mg	15 mg	20 mg	25 mg	30 mg	35 mg
Experimental	qe (mg·g^{-1})	40.00	39.55	38.80	38.13	37.01	35.82	34.62
Pseudo-First Order	k1 (min^{-1})	0.0556	0.0610	0.0574	0.0632	0.0628	0.0580	0.0619
	qe (mg·g^{-1})	24.86	27.06	25.75	26.87	21.33	21.58	20.42
	R^2	0.9787	0.9742	0.9738	0.9860	0.9687	0.9769	0.9803
Pseudo-Second Order	k2 (g·mg^{-1}·min^{-1})	0.0047	0.0050	0.0048	0.0049	0.0074	0.0060	0.0069
	qe (mg·g^{-1})	42.19	41.67	40.98	40.32	38.46	37.59	36.23
	R^2	0.9997	0.9998	0.9998	0.9998	0.9999	0.9999	0.9999
Intra-particle Diffusion	kid1 (mg·g^{-1}·min$^{-0.5}$)	2.2993	2.2163	2.2432	2.4187	1.815	2.034	1.9638

	C1	22.676	22.907	21.839	20.446	23.775	20.859	20.497
	R^2	0.9916	0.9702	0.9714	0.9636	0.8851	0.9726	0.9660
	kid2	0.5142	0.5176	0.5324	0.3479	0.3414	0.4296	0.2645
	C2	35.112	34.709	33.785	34.85	33.812	31.762	32.109
	R^2	0.9991	0.9644	0.9888	0.9958	0.9704	0.9965	0.9962

Table 3. Effect of initial RM21 dye concentration on kinetic parameters for RM21 adsorption on copper-doped ZnO nanocomposite decorated on kaolin

(Conditions: contact time: 90 min, adsorbent dosage: 30 mg·L⁻¹, temperature: 25°C)

Kinetic Model	**Parameter**	**15 mg**	**25 mg**	**35 mg**
Experimental	qe (mg·g^{-1})	23.98	35.82	42.63
Pseudo-First Order	k1 (min^{-1})	0.0622	0.0580	0.0537
	qe (mg·g^{-1})	15.49	21.58	25.86
	R^2	0.9839	0.9769	0.9735
Pseudo-Second Order	k2 (g·mg^{-1}·min^{-1})	0.0087	0.0060	0.0044
	qe (mg·g^{-1})	25.25	37.59	45.04
	R^2	0.9999	0.9999	0.9999
Intra-particle Diffusion	kid1 (mg·g^{-1}·min$^{-0.5}$)	1.5071	2.034	2.4531
	C1	13.145	20.859	24.129
	R^2	0.9651	0.9726	0.9842
	kid2	0.2319	0.4296	0.6788
	C2	21.79	31.762	36.215
	R^2	0.9958	0.9965	0.9957

As seen in Tables 2 and 3, the pseudo-second-order kinetic correlation coefficients were determined to be ~0.999 for all adsorbent amounts and initial dye concentrations. Furthermore, the qe values obtained from the experimental study were found to be similar to the theoretical qe values. The study was proven to be compatible with the pseudo-second-order kinetic model.

3.3.3. Intraparticle Diffusion

The intraparticle diffusion model proposed by Weber and Morris is based on the principle that adsorption occurs via mass transfer of adsorbate molecules onto the adsorbent. The linear form of this equation is written as follows (Weber and Morris 1963, Baldermann and Stamm 2022, Demir et al. 2022).

$qt=kid\sqrt{t}+C$ (12)

Here, k_{id} is the rate constant, and C is the model constants providing information about the boundary layer thickness. As shown in Figure 6c, kid and C values are obtained using the graph by plotting the change of qt value against $\sqrt{t}$. kid is calculated from the slope, and C is calculated from the point where the line intersects the y-axis of the graph.

In Figure 6c, for all seven concentrations, the plots show two-step multicollinearity. The first part of the linear plot is attributed to boundary layer diffusion, while the second part is attributed to intraparticle diffusion and chemical reaction. The fact that neither slope line passes through the origin indicates that film diffusion and intraparticle diffusion occur simultaneously (Nandi et al. 2009, Gad and El Sayed 2009). Tables 2 and 3 show the numerical values for kid1, kid2, C1, and C2 obtained from the lines in Figure 6c. These values indicate that the first step of adsorption, boundary layer diffusion, occurs faster (kid1>kid2) and relatively easier (C1<C2) than the second step, intraparticle diffusion.

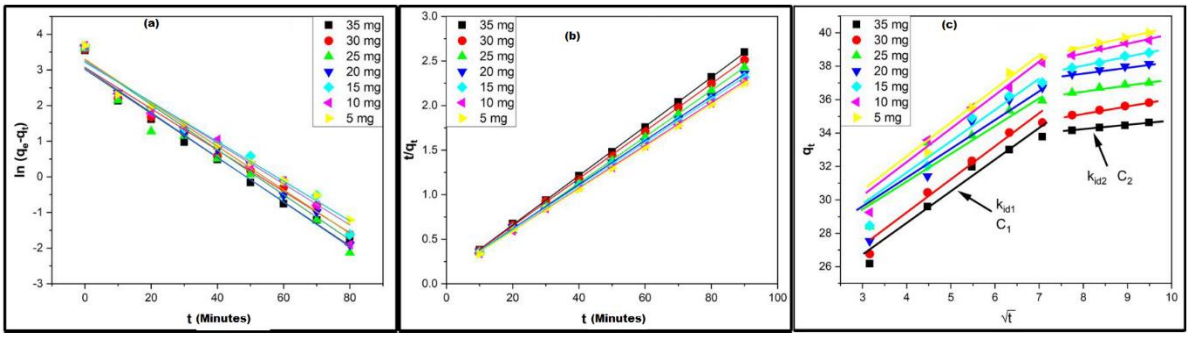

Figure 6. Kinetic models (a) Pseudo-first-order (b) Pseudo-second-order (c) Intraparticle diffusion

3.5. Evaluation of Post-adsorption SEM-EDX and FT-IR Data

The SEM-EDX and FT-IR spectra of RM21 dye after adsorption onto the copper-doped ZnO nanocomposite decorated on kaolin are presented in Figures 8 and 9, respectively. The post-adsorption SEM images indicate that the morphological structure of the copper-doped ZnO nanocomposite on the kaolin surface remained unchanged, with the presence of Cu-doped ZnO nanorods observed on the kaolin layers (Keleş Güner & Çağlar, 2020). The EDX spectrum shows Si, Al, O, and K elements originating from the kaolin, Cu, Zn, and O from the Cu-doped ZnO, and C, N, O, Cu, and S elements attributed to the adsorbed RM21 dye (Keleş Güner & Çağlar, 2020).

In the FT-IR spectrum of kaolin, bands at 3688, 3648, and 3618 cm^{-1} correspond to stretching vibrations of structural hydroxyl groups, while bands at 935, 910, and 788 cm^{-1} are related to bending vibrations of hydroxyl groups. Strong bands at 1024 and 996 cm^{-1} are attributed to Si–O–Si stretching vibrations, peaks at 750, 641, 523, and 456 cm^{-1} to bending vibrations of Si–O, Al–O–Si, and Si–O–Si, and the peak at 475 cm^{-1} is due to metal–oxygen stretching in the Cu-doped ZnO (Keleş Güner & Çağlar, 2020).

After the adsorption of RM21, characteristic IR peaks from the dye molecules were observed (Figure 9b). Peaks at 3690 and 3620 cm^{-1} correspond to O–H stretching vibrations of RM21, while the peak at 3446 cm^{-1} is attributed to both O–H and N–H stretching vibrations. The shoulder at 3020 cm^{-1} is assigned to aromatic C–H stretching, and peaks at 2923 and 2852 cm^{-1} correspond to aliphatic C–H stretching. Peaks at 1650, 1453, and 1384 cm^{-1} are associated with aromatic ring vibrations and C–H bending of RM21 (Figure 9b).

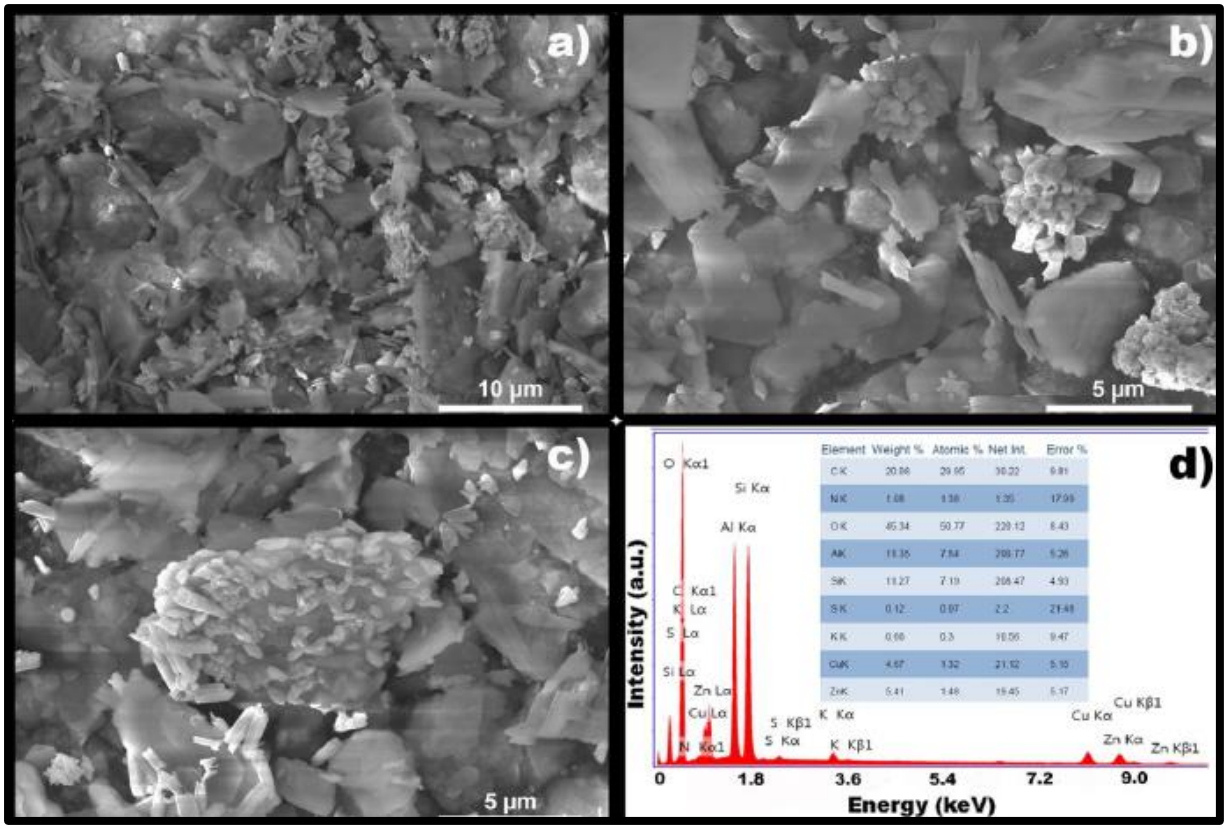

Figure 8. Post-adsorption characterization of RM21 dye on copper-doped ZnO nanocomposite decorated on kaolin: a–c) SEM images; d) EDX spectrum.

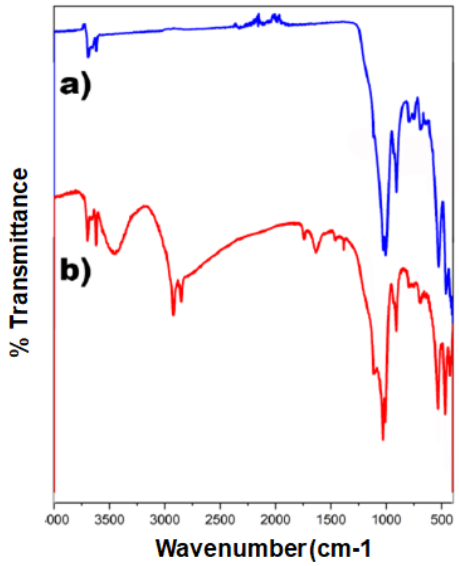

Figure 9. FT-IR spectra of copper-doped ZnO nanocomposite decorated on kaolin: a) before adsorption and b) after RM21 dye adsorption.

4. Conclusion

In this study, the copper-doped ZnO nanocomposite decorated on kaolin was successfully employed to remove RM21 dye from aqueous solutions. The results of the adsorption experiments indicated that the adsorption of RM21 onto the copper-doped ZnO nanocomposite on kaolin was best described by the Redlich-Peterson isotherm. Based on the correlation coefficients (R^2) of the isotherms, the

adsorption data fit the models in the following order: Redlich-Peterson > Langmuir > Jovanovich > Freundlich = Halsey > Temkin. Kinetic studies revealed that the adsorption process followed the pseudo-second-order kinetic model with a correlation coefficient of 0.9999 (R^2). Thermodynamic parameters ($\Delta G°$, $\Delta H°$, and $\Delta S°$) indicated that the adsorption process was feasible, endothermic, and spontaneous.

It can be concluded that the use of the copper-doped ZnO nanocomposite decorated on kaolin is an effective choice of adsorbent for the removal of RM21 dye from wastewater.

References

[1]. Ahmad, I., Kan, C., & Yao, Z. (2019). Photoactive cotton fabric for UV protection and self-cleaning. *RSC Advances, 9*, 18106–18114.

[2]. Al-Ghouti, M. A., & Da'ana, D. A. (2020). Guidelines for the use and interpretation of adsorption isotherm models: A review. *Journal of Hazardous Materials, 393*, 122383.

[3]. Alkan, M., Çelikçapa, S., Demirbaş, Ö., & Doğan, M. (2005). Removal of reactive blue 221 and acid blue 62 anionic dyes from aqueous solutions by sepiolite. *Dyes and Pigments, 65*, 251–259.

[4]. Al-Tohamy, R., Ali, S. S., Li, F., Okasha, K. M., Mahmoud, Y. A. G., Elsamahy, T., Jiao, H., Fu, Y., & Sun, J. (2022). A critical review on the treatment of dye-containing wastewater: Ecotoxicological and health concerns of textile dyes and possible remediation approaches for environmental safety. *Ecotoxicology and Environmental Safety, 231*, 113160.

[5]. Alswat, A. A., Al-shorifi, F. T., & Ali, S. L. (2022). Preparation of nanohybrid CuO-Fe3O4/zeolite nanocomposite as potential adsorbent for toxic As(V) and Pb(II) from water solution. *Iranian Journal of Materials Science and Engineering, 19*(3), 1–13.

[6]. Aksu, Z., & Isoglu, I. A. (2007). Use of dried sugar beet pulp for binary biosorption of Gemazol Turquoise Blue-G reactive dye and copper (II) ions: Equilibrium modeling. *Chemical Engineering Journal, 127*, 177–188.

[7]. Ayanda, O. S., Fatoki, O. S., Adekola, F. A., & Ximba, B. J. (2013). Activated carbon-fly ash-nanometal oxide composite materials: Preparation, characterization, and tributyltin removal efficiency. *Journal of Chemistry, 148129*, 1–10.

[8]. Baldermann, A., & Stamm, F. M. (2022). Effect of kinetics, pH, aqueous speciation and presence of ferrihydrite on vanadium (V) uptake by allophanic and smectitic clays. *Chemical Geology, 607*, 121022.

[9]. Bamfield, P. (2001). *Chromic phenomena: The technological applications of colour chemistry*. Cambridge, UK: Royal Society of Chemistry.

[10]. Bayramoğlu, G., Altintaş, B., & Arica, M. Y. (2009). Adsorption kinetics and thermodynamic parameters of cationic dyes from aqueous solutions by using a new strong cation-exchange resin. *Chemical Engineering Journal, 152*(2–3), 339–346.

[11]. Bayramoğlu, G., Kunduzcu, G., & Arica, M. Y. (2020). Preparation and characterization of strong cation exchange terpolymer resin as effective adsorbent for removal of disperse dyes. *Polymer Engineering & Science, 60*(1), 192–201.

[12]. Bensalah, J., Habsaoui, A., Dagdag, O., Lebkiri, A., Ismi, I., Rifi, E. H., Warad, I., & Zarrouk, A. (2021). Adsorption of a cationic dye (Safranin) by artificial cationic resins Amberlite® IRC-50: Equilibrium, kinetic and thermodynamic study. *Chemical Data Collections, 35*, 100756.

[13]. Bilińska, L., Blus, K., Gmurek, M., & Ledakowicz, S. (2019). Coupling of electrocoagulation and ozone treatment for textile wastewater reuse. *Chemical Engineering Journal, 358*, 992–1001.

[14]. Binaeian, E., Zadvarzi, S. B., & Yuan, D. (2020). Anionic dye uptake via composite using chitosan-polyacrylamide hydrogel as matrix containing TiO2 nanoparticles; comprehensive adsorption studies. *International Journal of Biological Macromolecules, 162*, 150–162.

[15]. Boulika, H., El Hajam, M., Nabih, M. H., Karim, I. R., Kandri, N. I., & Zerouale, A. (2023). Definitive screening design applied to cationic & anionic adsorption dyes on almond shells activated carbon: Isotherm, kinetic and thermodynamic studies. *Materials Today: Proceedings, 72*, 3336–3346.

[16]. Broadbent, A. D. (2001). *Basic principles of textile coloration*. West Yorkshire, UK: Society of Dyers and Colourists.

[17]. Chandrabose, G., Dey, A., Gaur, S. S., Pitchaimuthu, S., Jagadeesan, H., Braithwaite, N. J., Selvaraj, V., Kumar, V., & Krishnamurthy, S. (2021). Removal and degradation of mixed dye pollutants by integrated adsorption-photocatalysis technique using 2-D MoS2/TiO2 nanocomposite. *Chemosphere, 279*, 130467.

[18]. De Gisi, S., Lofrano, G., Grassi, M., & Notarnicola, M. (2016). Characteristics and adsorption capacities of low-cost sorbents for wastewater treatment: A review. *Sustainable Materials and Technologies, 9*, 10–40.

[19]. Demir, B., & Kalpaklı, Y. (2020). İşlem görmemiş Kütahya CaBentonitinin Bazik Mavi 41 (BB41) Adsorpsiyon Karakteristiğinin İncelenmesi. *Iğdır Üniversitesi Fen Bilimleri Enstitüsü Dergisi, 10*(1), 309–319.

[20]. Demir, Ö., Gök, A., & Kırbaşlar, Ş. A. (2022). Optimization of protocatechuic acid adsorption onto weak basic anion exchange resins: Kinetic, mass transfer, isotherm, and thermodynamic study. *Biomass Conversion and Biorefinery, 138*, 1–12.

[21]. El-Bindary, A. A., Abd El-Kawi, M. A., Hafez, A. M., Rashed, I. G. A., & Aboelnaga, E. E. (2016). Removal of reactive blue 19 from aqueous solution using rice straw fly ash. *Journal of Materials and Environmental Science, 7*(3), 1023–1036.

[22]. El-Desouky, M. G., El-Bindary, A. A., & El-Bindary, M. A. (2021). Low-temperature adsorption study of carbon dioxide on porous magnetite nanospheres iron oxide. *Biointerface Research in Applied Chemistry, 12*(5), 6252–6268.

[23]. Eren, E., Çağlar, B., Eren, B., & Tabak, A. (2010). Equilibrium and kinetic studies on the removal of basic dye using raw and thermal-activated Fatsa bentonite. *Fresenius Environmental Bulletin, 19*(5), 773–782.

[24]. Eskandari, P., Farhadian, M., Nazar, A. R. S., & Goshadrou, A. (2021). Cyanide adsorption on activated carbon impregnated with ZnO, Fe2O3, TiO2 nanometal oxides: A comparative study. *International Journal of Environmental Science and Technology, 18*, 297–316.

[25]. Ewis, D., Ba-Abbad, M. M., Benamor, A., Mahmud, N., Nasser, M., El-Naas, M., & Mohammad, A. W. (2022). Adsorption of 4-nitrophenol onto iron oxide bentonite nanocomposite: Process optimization, kinetics, isotherms and mechanism. *International Journal of Environmental Research, 16*, 23.

[26]. Fadillah, G., Yudha, S. P., Sagadevan, S., Fatimah, I., & Muraza, O. (2020). Magnetic iron oxide/clay nanocomposites for adsorption and catalytic oxidation in water treatment applications. *Open Chemistry, 18*, 1148–1166.

[27]. Gad, H. M. H., & El-Sayed, A. A. (2009). Activated carbon from agricultural by-products for the removal of Rhodamine-B from aqueous solution. *Journal of Hazardous Materials, 168*, 1070–1081.

[28]. Gan, W., Shang, X., Li, X. H., Zhang, J., & Fu, X. (2019). Achieving high adsorption capacity and ultrafast removal of methylene blue and Pb^{2+} by graphene-like TiO_2@C. *Colloids and Surfaces A, 561*, 218–225.

[29]. Ghaffar, A., Adeel, S., Habib, N., Jalal, F., Atta-ul-Haq, Munir, B., Ahmad, A., Jahangeer, M., & Jamil, Q. (2019). Effects of microwave radiation on cotton dyeing with Reactive Blue 21 dye. *Polish Journal of Environmental Studies, 28*(3), 1687–1691.

[30]. Gholitabar, S., & Tahermansouri, H. (2017). Kinetic and multi-parameter isotherm studies of picric acid removal from aqueous solutions by carboxylated multi-walled carbon nanotubes in the presence and absence of ultrasound. *Carbon Letters, 22*, 14–24.

[31]. Haladu, S. A. (2022). Highly efficient adsorption of malachite green dye onto a cross-linked pH-responsive cycloterpolymer resin: Kinetic, equilibrium and thermodynamic studies. *Journal of Molecular Liquids, 357*, 119115.

[32]. Hamad, H. N., & Idrus, S. (2022). Recent developments in the application of bio-waste-derived adsorbents for the removal of methylene blue from wastewater: A review. *Polymers, 14*, 783.

[33]. Hassan, M. M., & Carr, C. M. (2018). A critical review on recent advancements of the removal of reactive dyes from dyehouse effluent by ion-exchange adsorbents. *Chemosphere, 209*, 201–219.

[34]. Kalam, S., Abu-Khamsin, S. A., Kamal, M. S., & Patil, S. (2021). Surfactant adsorption isotherms: A review. *ACS Omega, 6*, 32342–32348.

[35]. Karaoğlu, M. H., Doğan, M., & Alkan, M. (2009). Removal of cationic dyes by kaolinite. *Microporous and Mesoporous Materials, 122*, 20–27.

[36]. Keleş Güner, E., & Çağlar, B. (2020). CuxZn(1-x)O nanoparticles decorated kaolin nanocomposite: Synthesis, characterization, and photocatalytic activity. *Erzincan Üniversitesi Fen Bilimleri Enstitüsü Dergisi, 13*(2), 369–383.

[37]. Khan, T. A., Khan, E. A., & Shahjahan. (2015). Removal of basic dyes from aqueous solution by adsorption onto binary iron-manganese oxide coated kaolinite: Non-linear isotherm and kinetics modelling. *Applied Clay Science, 107*, 70–77.

[38]. Kızıltaş, H. (2022). Production of highly effective adsorbent from tea waste, and its adsorption behaviors and characteristics for the removal of Rhodamine B. *International Journal of Environmental Analytical Chemistry, 1*, 1–20.

[39]. Kibanova, D., Sleiman, M., Cervini-Silva, J., & Destaillats, H. (2012). Adsorption and photocatalytic oxidation of formaldehyde on a clay-TiO_2 composite. *Journal of Hazardous Materials, 211–212*, 233–239.

[40]. Kiełbasa, K., Kaminska, A., Niedoba, O., & Michalkiewicz, B. (2021). CO_2 adsorption on activated carbons prepared from molasses: A comparison of two and three parametric models. *Materials, 14*, 7458.

[41]. Kul, A. R., Benek, V., Erge, H., Demirci, S., & Adıgüzel, V. (2022). Adsorption isotherm study of malachite green dye on pumice. *Kafkas Üniversitesi Fen Bilimleri Enstitüsü Dergisi, 15*(1), 12–19.

[42]. Kumbhar, P., Narale, D., Bhosale, R., Jambhale, C., Kim, J. H., & Kolekar, S. (2022). Synthesis of tea waste/Fe_3O_4 magnetic composite (TWMC) for efficient adsorption of crystal violet dye:

Isotherm, kinetic and thermodynamic studies. *Journal of Environmental Chemical Engineering, 10*, 107893.

[43]. Küçük, İ. (2021). Methylene blue adsorption capacity and coherent isotherm model of commercial activated carbon. *Cumhuriyet Science Journal, 42*(4), 843–851.

[44]. Lagergren, S. (1898). Zur theorie der sogenannten adsorption gelöster stoffe. *Kungliga Svenska Vetenskapsakademiens Handlingar, 24*, 1–39.

[45]. Lellis, B., Fávaro-Polonio, C. Z., Pamphile, J. A., & Polonio, J. C. (2019). Effects of textile dyes on health and the environment and bioremediation potential of living organisms. *Biotechnology Research and Innovation, 3*(2), 275–290.

[46]. Liu, S., Li, B., Qi, P., Yu, W., Zhao, J., & Liu, Y. (2019). Performance of freshly generated magnesium hydroxide (FGMH) for reactive dye removal. *Colloid and Interface Science Communications, 28*, 34–40.

[47]. Lu, C., & Chiu, H. (2006). Adsorption of zinc(II) from water with purified carbon nanotubes. *Chemical Engineering Science, 61*(4), 1138–1145.

[48]. Luo, C., Yao, W., & Gao, X. (2022). Degradation of a Reactive Orange 16 in textile wastewater treatment using CuO/ZnO nanocomposite as photocatalyst. *International Journal of Electrochemical Science, 17*, 220732.

[49]. Mahmood, R. S. (2022). The uptake of Eriochrome Black T dye from wastewater utilizing synthesized cadmium sulfide nanoparticles. *Egyptian Journal of Chemistry, 65*(6), 699–706.

[50]. Markandeya, Mohan, D., & Prasad Shukla, S. (2022). Hazardous consequences of textile mill effluents on soil and their remediation approaches. *Cleaner Engineering and Technology, 7*, 100434.

[51]. Mia, R., Selim, M., Shamim, A., Mugdho, M. C., Sultana, S., Armin, M., & Naznin, H. (2019). Review on various types of pollution problems in textile dyeing & printing industries of Bangladesh and recommendations for mitigation. *Journal of Textile Engineering, 5*, 220–226.

[52]. Muthuvela, A., Jothibasa, M., & Manoharan, C. (2020). Effect of chemically synthesized compared to biosynthesized ZnO-NPs using Solanum nigrum leaf extract and their photocatalytic, antibacterial and in vitro antioxidant activity. *Journal of Environmental Chemical Engineering, 8*, 103705.

[53]. Nandi, B. K., Goswami, A., & Purkait, M. K. (2009). Removal of cationic dyes from aqueous solutions by kaolin: Kinetic and equilibrium studies. *Applied Clay Science, 42*, 583–590.

[54]. Nasar, A., & Mashkoor, F. (2019). Application of polyaniline-based adsorbents for dye removal from water and wastewater: A review. *Environmental Science and Pollution Research, 26*(6), 5333–5356.

[55]. Naseem, T., & Durrani, T. (2021). The role of some important metal oxide nanoparticles for wastewater and antibacterial applications: A review. *Environmental Chemistry and Ecotoxicology, 3*, 59–75.

[56]. Nazifa, T. H., Habba, N., Salmiati, Aris, A., & Hadibarata, T. (2017). Adsorption of Procion Red MX-5B and Crystal Violet dyes from aqueous solution onto corncob activated carbon. *Journal of the Chinese Chemical Society, 65*(2), 259–270.

[57]. Ncibi, M. C., Mahjoub, B., & Seffen, M. (2007). Adsorptive removal of textile reactive dye using *Posidonia oceanica* (L.) fibrous biomass. *International Journal of Environmental Science and Technology, 4*(4), 433–440.

[58]. Özdemir, A. O. (2015). *Pamuk liflerinin renklendirilmesinde boyama verimi ve kinetiğinin araştırılması* (Doctoral dissertation, Erciyes Üniversitesi, Fen Bilimleri Enstitüsü).

[59]. Özdemir, A. O., & Tutak, M. (2016). Reactive Black 5 dyeing behavior on cotton fabric: K/S color yield, fixation, and fastness properties. *Niğde Üniversitesi Mühendislik Bilimleri Dergisi, 5*(1), 83–88.

[60]. Pala, S. L., Mekala, S., & Ravindhranath, K. (2022). Novel adsorbents for simultaneous extraction of lead and cadmium ions from polluted water: Based on active carbon, nanometal (Zr-Ce-Sm)-mixed oxides and iron-alginate beads. *Biomass Conversion and Biorefinery*. Advance online publication. https://doi.org/10.1007/s13399-022-03316-4

[61]. Patra, T., Mohanty, A., Singh, L., Muduli, S., Parhi, P. K., & Sahoo, T. R. (2022). Effect of calcination temperature on morphology and phase transformation of MnO_2 nanoparticles: A step towards green synthesis for reactive dye adsorption. *Chemosphere, 288*, 132472.

[62]. Rais, A. (2009). Studies on adsorption of crystal violet dye from aqueous solution onto coniferous pinus bark powder (CPBP). *Journal of Hazardous Materials, 171*, 767–773.

[63]. Rind, I. K., Tuzen, M., Sarı, A., Lanjwani, M. F., Memon, N., & Saleh, T. A. (2023). Synthesis of TiO_2 nanoparticles loaded on magnetite nanoparticles modified kaolinite clay (KC) and their efficiency for As(III) adsorption. *Chemical Engineering Research and Design, 191*, 523–536.

[64]. Saeed, T., Naeem, A., Din, I. U., Farooq, M., Khan, I. W., Hamayun, M., Malik, T. (2022). Synthesis of chitosan composite of metal-organic framework for the adsorption of dyes; kinetic and thermodynamic approach. *Journal of Hazardous Materials, 427*, 127902.

[65]. Saloğlu, D. (2019). Mikro kirletici naproksenin atık sulardan Spirulina platensis ile modifiye edilmiş kitosan-polivinilalkol biyokompozitleri ile adsorpsiyonu. *BEÜ Fen Bilimleri Dergisi, 8*(2), 506–520.

[66]. Sarı, A., & Soylak, M. (2006). Equilibrium and thermodynamic studies of stearic acid adsorption on Celtek clay. *Journal of the Serbian Chemical Society, 72*(5), 485–494.

[67]. Senthil Rathi, B., & Senthil Kumar, P. (2021). Application of adsorption process for effective removal of emerging contaminants from water and wastewater. *Environmental Pollution, 280*, 116995.

[68]. Simonic, M., Flucher, V., Luxbacher, T., Vesel, A., & Zemljic, L. F. (2022). Adsorptive removal of heavy metal ions by waste wool. *Journal of Natural Fibers*, 1–14.

[69]. Stengl, V., & Králová, D. (2011). TiO_2/ZnS/CdS nanocomposite for hydrogen evolution and Orange II dye degradation. *International Journal of Photoenergy, 2011*, 532578.

[70]. Sun, Y. F., Liu, S. B., Meng, F. L., Liu, J. Y., Jin, Z., Kong, L. T., & Liu, J. H. (2012). Metal oxide nanostructures and their gas sensing properties: A review. *Sensors, 12*, 2610–2631.

[71]. Tekin, D., Tekin, T., & Kızıltaş, H. (2020). Synthesis and characterization of TiO_2 and Ag/TiO_2 thin-film photocatalysts and their efficiency in the photocatalytic degradation kinetics of Orange G dyestuff. *Desalination and Water Treatment, 198*, 376–385.

[72]. Vaghela, N. R., & Nath, K. (2020). Reduced graphene oxide coated graphite electrodes for treating Reactive Turquoise Blue 21 rinse water using an indirect electro-oxidation process. *SN Applied Sciences, 2*, 1839.

[73]. Velusamy, S., Roy, A., Sundaram, S., & Mallick, T. K. (2021). A review on heavy metal ions and containing dyes removal through graphene oxide-based adsorption strategies for textile wastewater treatment. *Chemical Record, 21*, 1570–1610.

[74]. Viana, T., Henriques, B., Ferreira, N., Pinto, R. J. B., Monteiro, F. L. S., & Pereira, E. (2023). Insight into the mechanisms involved in the removal of toxic, rare earth and platinum elements from complex mixtures by *Ulva* sp. *Chemical Engineering Journal, 453*, 139630.

[75]. Weber, J. W. J., & Morriss, J. C. (1963). Kinetics of adsorption on carbon from solution. *Journal of the Sanitary Engineering Division, ASCE, 89*, 31–60.

[76]. Xu, R., Zou, W., Rao, B., Zhao, W., Wang, T., & Zhang, Z. (2023). In situ kinetics and flocs conformation studies of kaolinite flocculated by Chi-g-CPAM. *International Journal of Minerals, Metallurgy and Materials, 30*(5), 813–823.

[77]. Xu, S., Niu, X., Hou, Z., Gao, C., Lu, J., Pang, Y., & Joshy, K. (2020). A multifunctional gelatine–quaternary ammonium copolymer: An efficient material for reducing dye emission in leather tanning process by superior anionic dye adsorption. *Journal of Hazardous Materials, 383*, 121142.

[78]. Yagub, M. T., Sen, T. K., Afroze, S., & Ang, H. M. (2014). Dye and its removal from aqueous solution by adsorption: A review. *Advances in Colloid and Interface Science, 209*, 172–184.

[79]. Zewde, D., & Geremew, B. (2022). Removal of Congo red using *Vernonia amygdalina* leaf powder: Optimization, isotherms, kinetics, and thermodynamics studies. *Environmental Pollutants and Bioavailability, 34*(1), 88–101.

[80]. Zheng, S., Sun, Z., Park, Y., Ayoko, G. A., & Frost, R. A. (2013). Removal of bisphenol A from wastewater by Ca-montmorillonite modified with selected surfactants. *Chemical Engineering Journal, 234*, 416–422.

[81]. Zhou, Y., Lu, J., Zhou, Y., & Liu, Y. (2019). Recent advances for dyes removal using novel adsorbents: A review. *Environmental Pollution, 252*, 352–365